Journal of Thermal Analysis and Calorimetry (2018) 132:813–822
https://doi.org/10.1007/s10973-018-7004-6

Optimization of mechanical properties of complex, two-stage heat treatment of Cu–Ni (Mn, Mo) austempered ductile iron

Andrzej Gazda[1] · Małgorzata Warmuzek[1] · Adam Bitka[1]

Received: 25 August 2017 / Accepted: 15 January 2018 / Published online: 25 January 2018

Abstract
The aim of the study was to design and optimize the complex, two-step heat treatment of Cu–Ni (Mn, Mo) ductile iron. A method for the formation and investigation of austempered ductile iron (ADI) by means of complex two-step and as comparative, standard one-step heat treatments has been developed, using quenching dilatometer. Investigations of proceeding phase transformations using differential dilatometric and DSC analysis supported by microstructural observations, hardness and austenite volume measurements have been carried out. An analysis of the temperature sequence of the ausferrite decomposition in the one-step and two-step ADI was performed, which allowed for the separation and identification of the effects responsible for the carbon-enriched austenite decomposition. A quantitative relationship was established between basic dimensional effects revealed on the differential dilatometric curve of ausferrite decomposition, which enables prognosis and optimization of the parameters of complex ADI heat treatment variants. Verification tests were performed on a stand equipped with salt furnaces enabling a quick transfer of samples from one bath to another without changing their initial temperature. Optimization of the two-step ADI heat treatment with the use of quantitative dilatometric analysis of the ausferrite decomposition, allowed to obtain for the temperature step-down heat treatment 390 °C/15, 20 min ≫ 270 °C/130 min the excellent mechanical properties, unattainable by means of standard 1-step ADI heat treatment.

Keywords ADI · Ausferrite · Thermal analysis · Dilatometry · DSC · SEM · Mechanical properties

Introduction

Austempered ductile iron (ADI) is a ductile iron subjected to the heat treatment consisting of austenitizing and quenching followed by an isothermal transformation—austempering. ADI has a good machinability, wear resistance, damping capacity and excellent mechanical properties—toughness and fatigue strength accompanied by high strength-to-weight ratio.

The structure and mechanical properties of ADI depend on the sequence of phase transformations during the austempering. In the first stage of austenite isothermal decomposition, ausferrite consisting of fine acicular ferrite α_{ac} and metastable reacted carbon-saturated austenite $\gamma_{s'}(C)$ is created. As a result of further step of austempering within processing window, optimum ausferrite with maximum amount of fine acicular ferrite α_{sac} and reacted stable, carbon-saturated austenite $\gamma_s(C)$ is formed. Austempering heat treatment parameters should prevent martensite or carbides formation. Extending the time of isothermal transformation beyond the processing window leads to decomposition of carbon-rich austenite to ferrite and carbides.

ADI was the subject of many studies dedicated to optimization of its mechanical and utility properties, especially for new applications in the special work conditions. There are many publications, e.g., [1–6], concerning description and identification of the microstructural components, selection of optimum austenitization and austempering parameters, role of alloying elements and other problems related to standard one-step ADI heat treatment with aim to optimize mechanical and utility properties. Thermal stability of ausferrite and its

✉ Andrzej Gazda
andrzej.gazda@iod.krakow.pl

[1] Foundry Research Institute, 73 Zakopianska St., 30-418 Kraków, Poland

decomposition at elevated temperatures are also of interest to many works [7–14]. Retained austenite present in ADI in the reacted stable and unreacted metastable forms may be subjected to martensitic transformation proceeding at different stages of austempering, especially while final cooling to the room temperature. A description of problems related to these harmful phenomena decreasing mechanical properties, mainly ductility, can be found, for example, in the publications [1, 12, 15–18].

Objective in this study was to optimize a complex two-step ADI heat treatment, based on the analysis of the fundamental one-step austempering process. This complex type of ADI heat treatment has a rich bibliography [19–28]. The opinion that complex heat treatment does enable better mechanical properties, both R_m and A, than those achieved due to standard one-step austempering is established.

The approach presented in this paper is based on the weaker assumption that complex heat treatment enables obtaining better mechanical properties of ADI which are not possible to obtain in standard, one-step heat treatment. It means that this complex heat treatment modifies the strength–elongation relationship, $R_m = F(A)$, in such a way that new function F' satisfies the condition that $F'(A) > F(A)$ at the same strength or $F''(R_m) > F(R_m)$ at the same ductility.

Thus, two variants of the austempering course will be considered. The step-up variant in which the preliminary stage takes place at a lower temperature guarantees high strength. The final stage at higher temperature allows the martensite tempering and additional austenite saturation with carbon due to the faster carbon diffusion at elevated temperature.

The step-down variant in which the initial stage is carried out at a higher temperature allows austenite to be saturated with carbon and prevents the harmful formation of martensite from untransformed austenite. The final stage at lower temperature inhibits ausferrite growth and reduces the feathered morphology of acicular ferrite.

Design of austempered ductile iron with specific properties is based on the direct analysis of diffusionless (shear mechanism) and the diffusive phase transformation's sequence leading to the ausferrite formation and the indirect analysis, involving the study a sequence of thermal decomposition of phases produced in austempering process. From the experimental point of view, in the laboratory scale, direct analysis requires to perform a specified heat treatments and at the same time allowing to record the structure-sensitive physical quantities in device and determine the correlation between the basic processing parameters and thermophysical properties. Complementary to this approach is the indirect (inverse) analysis carried out by means of non-isothermal thermal analysis methods. In this approach very useful is the analysis of the sequence of phase transformations proceeding during heating, reflecting decomposition of metastable phases produced during ADI heat treatment. First-order phase transformations, which are considered, are described by changes of entropy (or enthalpy) ($\Delta H \neq 0$) and volume ($\Delta V \neq 0$), so both calorimetric (DSC) and dilatometric methods are suitable and very useful here [29, 30].

Results obtained by these methods will be completed with the microscopic observations of the microstructure evolution as affected by controlled heat treatment. The microstructure effects ascribed to measured thermophysical properties (enthalpy and volume) will be the base of analyzing the decomposition path of the initial phase constituents.

Experimental

Thermal analysis methods were used to produce the test material as well as to analyze the phase transformations accompanying the decomposition processes of the ausferrite during controlled temperature changes.

High Speed Quenching Dilatometer Linseis RITA L78, which allows high heating/cooling rates up to 150 K s^{-1} (induction heating), has been used to produce relatively small cylindrical samples 10 mm long and 3 mm in diameter with a different ausferrite structure and for the construction of CCT and TTT diagrams. Accurate sample temperature measurement is obtained by means of K-type thermocouple welded to the sample.

The dilatometric analyses of the ausferrite were performed in a Netzsch DIL 402C dilatometer in the range from ambient temperature to approximately 750 °C (below the A_{c1} temperature) with a heating rate $q = 5$ K min^{-1} in a dynamic Ar 5.0 protection atmosphere.

The Netzsch DSC 404C Differential Scanning Calorimeter was used for calorimetric studies of the ausferrite decomposition processes. Temperature and sensitivity calibration of the device was performed using the melting enthalpies of the pure elements In, Sn, Zn, Al, Ag, Au. DSC measurements were carried out from ambient to ca 750 °C, using varying heating rates (2–20 K min^{-1}) in Ar 5.0 protective atmosphere. Each DSC measurement was repeated under identical conditions, and the resulting physical baseline curve was subtracted from the first curve obtained for the as-austempered sample, giving resulting DSC curve.

The HV30/15 Vickers hardness measurements and the austenite volume fraction evaluated using a Ferrikomp technical tool, operating on the principle eddy current to determine the ferrite content, were used as parameters to characterize the heat treatment effects.

The mass fraction of carbon-enhanced austenite and carbon content in austenite was determined using the Bruker D8 Discover X-ray diffractometer.

Examinations of the alloy microstructure and morphology of graphite were made by means of light metallographic microscope Axio Observer.Z1m. Graphite was observed on the polished metallographic cross sections, while the microstructure morphology on those etched with 4% nital reagent.

More detailed observations of the alloy microstructure and phase constituents morphology were carried out by means of scanning electron microscope Scios FEI.

Samples after selected heat treatment variants were subjected to a static tensile test at room temperature using EU-20 strength machine (0–100 kN).

The principle of conducting minimum two measurement series for the given treatment and type of analysis and differentiation of the heat treatment technique (laboratory − dilatometer/traditional − salt furnaces) was applied in the work where possible. Each measuring point is the average of three measurements carried out under the same conditions. Due to the methodology of thermal analysis studies, the measurement results are subjected to type B uncertainty.

Material for the study was a ductile cast iron alloyed with Ni, Cu, Mo and Mn, obtained in a foundry induction furnace. Table 1 shows the chemical composition of the examined alloy [31].

The matrix of the as-cast ductile iron consists of 96% pearlite and well-shaped graphite (70%VI6 + 30%V6 acc. to PN-EN ISO 945-1:2009) characterized by 8.1% volume fraction and relatively small number of spheroids 60 per mm^2.

Heat treatment

Two types of ADI heat treatments of spheroidal cast iron, one step and two steps were performed. Selection of the optimal heat treatment parameters was based on the analysis of CCT and TTT diagrams, supported by metallographic studies and hardness measurements, summarized in the previous paper [31]. The following values of ADI heat treatment parameters were established, after austenitization at 910 °C for 40 min and cooling down to austempering temperature at the cooling rate 100 K s^{-1}.

One-step heat treatment—austempering at 270, 310, 350 and 390 °C for 150, 120, 90 and 60 min, respectively,

Two-step heat treatment

- Austempering at 270, 310 °C in a few short time intervals, necessary to proceed from 5% to approx. 40% of transformation, then completed at 350, 390 °C (step-up) for a time specified by TTT diagram;
- Austempering at 350, 390 °C in a few short time intervals, necessary to proceed from 5% to approx. 40% of transformation, then completed at 270, 310 °C (step-down) for a time specified by TTT diagram.

The materials for dilatometric, DSC and structural investigations were manufactured under laboratory conditions in the Linseis L78 RITA quenching dilatometer and in the salt furnace stand. In a first case, dimensional changes (linear or volumetric) accompanying the phase transitions induced by the various types or segments of heat treatment useful for quantitative analysis, were additionally recorded.

Characteristics of ADI material

After heat treatment, non-destructive tests were conducted, and HV30 hardness and carbon-enriched austenite fraction V_a in the alloy were determined, as forecasting and indicative parameters of the basic mechanical properties of ADI—tensile strength R_m and ductility (elongation) A.

Figure 1a, b presents dependence of HV30 and V_a on austempering temperature for one-step heat treatment and calculated relation between hardness and austenite fraction, respectively.

Figure 2a, b presents dependence of HV30 and V_a on dwell time of the initial temperature step of a two-step heat treatment. For the step-up ADI treatment, an increase in the first-stage duration is accompanied by the increase in HV30 and a decrease in V_a. For the step-down case of this complex heat treatment, prolonged time of the initial stage causes an increase in V_a and a decrease in HV30, which is qualitatively in agreement with the results for the one-step ADI heat treatment.

Morphology of the alloy matrix after different variants of the heat treatment, observed by means of the scanning electron microscope, is presented in Fig. 3a–d.

One can see that alloy microstructure formed due to heat treatment was affected by its parameters, temperature, time

Table 1 Chemical composition of the examined alloy/wt%

C	Si	Ni	Cu	Mn	Mo	Mg	Cr	Al	P	S
3.66	2.38	0.85	0.53	0.21	0.16	0.07	0.05	0.013	0.042	0.032

and heat treating mode. In the specimens after one-step treatment, an increase in the austempering temperature resulted in a growth of grains (Fig. 3a, b) and in the thickness of ferrite plates/needles. The two-step treatment application, of the both variants, resulted in the more homogeneous microstructure morphology, especially more uniform ferrite plates/needles dispersion in both examined specimen (Fig. 3c, d). However, dispersion of ferrite plates/needles was slightly higher after step-down treatment (Fig. 3c) in comparison with that observed after step-up variant (Fig. 3d).

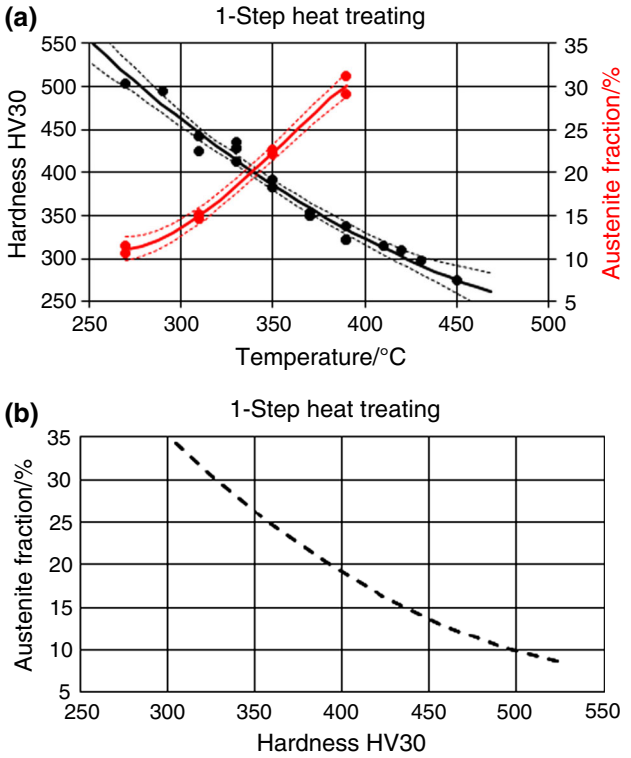

Fig. 1 One-step heat treatment; dependence of HV30 and V_a on the temperature of austempering (**a**), calculated relation between V_a and HV30 (**b**)

Decomposition of ADI

The obtained ADI material, defined by means of a specific heat treatment, has been subjected to controlled destruction, i.e., decomposition studies combined with recording of dimensional (differential dilatometric analysis) and thermal (DSC) effects.

Figure 4a shows the recorded sequence of dimensional changes accompanying the decomposition process of the ausferrite after one-step treatment carried out at various constant temperatures. Figure 4b depicts the corresponding exothermic effects recorded under similar conditions by DSC curves, less sensitive to structural changes occurring during heating of ADI.

With increasing austempering temperature, the main dimensional (volume) effect decreases and exothermal DSC effect increases, indicating the decomposition of austenite. In addition, the DSC peaks show a shift toward the higher temperature which may suggest greater thermal stability of high-temperature (upper) ausferrite.

The deconvolution of the recorded, complex differential dilatometric α (Alpha) curves by PeakFit 4.12 has been performed. Software allows peaks separation by the selection and fitting of analytical functions, determination of their temperatures and calculation of the relative dimensional changes ($\Delta L/L_o$) of peaks and provides statistics of fitting.

Generated by software, exemplary differential dilatometric curves—as measured (upper side) and deconvoluted Alpha* = $(dL/dT)/L_o$ − baseline(T), elaborated for decomposition processes after one-step and two-step-down heat treatments are shown in Figs. 5a, b and 6a, b, respectively.

Figure 7a shows an enlarged section of Fig. 4a to facilitate the interpretation of recorded curves.

Negative dimensional effect **0** recorded at a temperature of about 100–170 °C is the result of the tempering of as-quenched martensite present in structure, transformation of

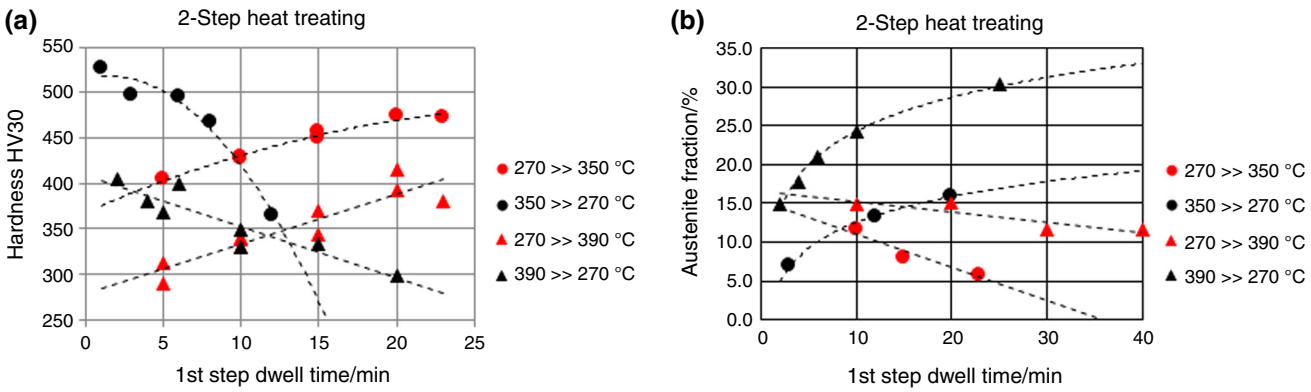

Fig. 2 Two-step heat treatment; dependence of HV30 (**a**) and V_a (**b**) on dwell time of the initial temperature step

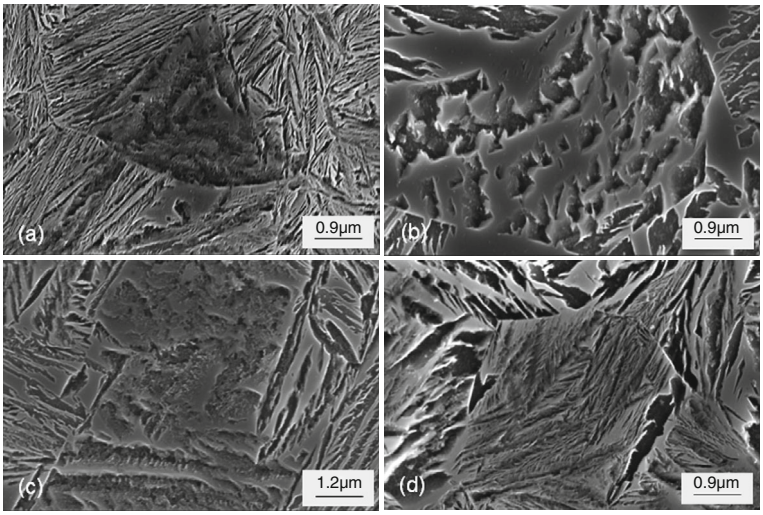

Fig. 3 Microstructure of the examined alloy after heat treatment, SEM; one-step austempering at 270 °C (**a**), one-step austempering at 390 °C (**b**), two-step (up) austempering 270 ≫ 390 °C (**c**), two-step (down) austempering 390 ≫ 270 °C (**d**)

supersaturated tetragonal ferrite into supersaturated acicular ferrite (α_{sac}) + coherent carbides and gradual stress relaxation [14, 15]. The positive volumetric effect **1** of the DSC curve corresponds to a broad exothermic effect occurring in a relatively wide temperature range of 250–400 °C and reflects, as indicated by its positive sign, the decomposition of the unstable austenite with a low carbon content. The magnitude of this effect is clearly

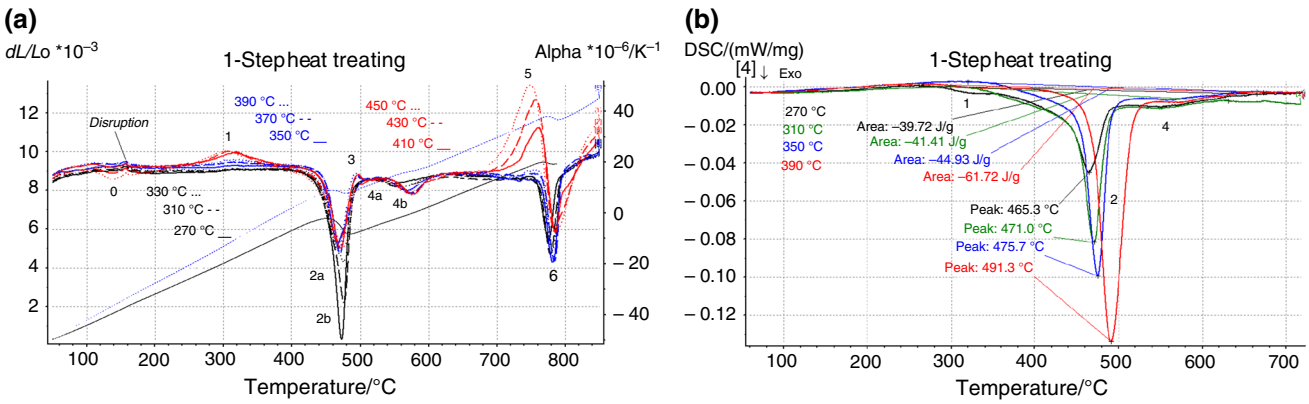

Fig. 4 Decomposition of one-step ADI heat treatment; differential dilatometric curves (**a**), DSC curves (**b**)

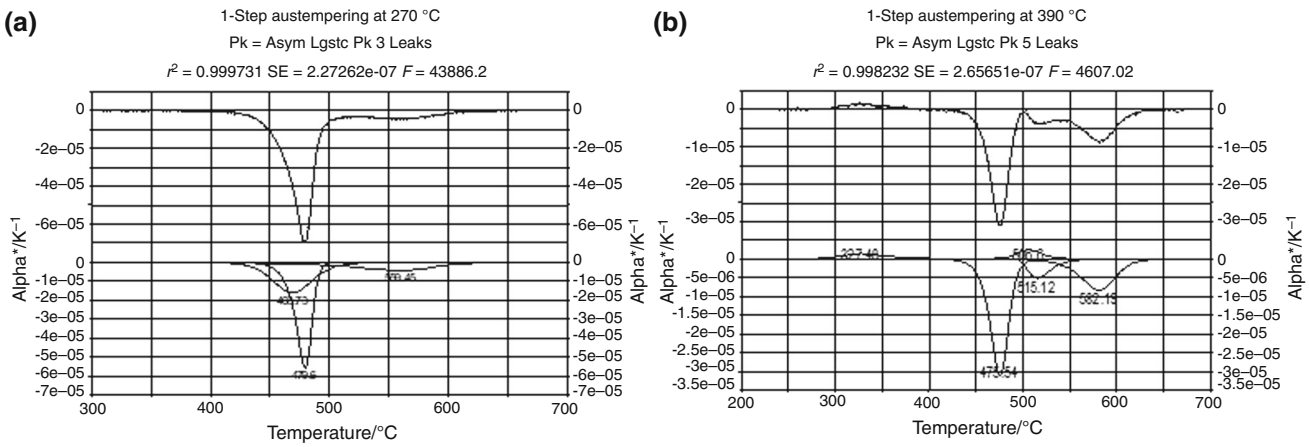

Fig. 5 Deconvolution of dilatometric curves—decomposition after one-step heat treatment performed at 270 °C (**a**) and 390 °C (**b**)

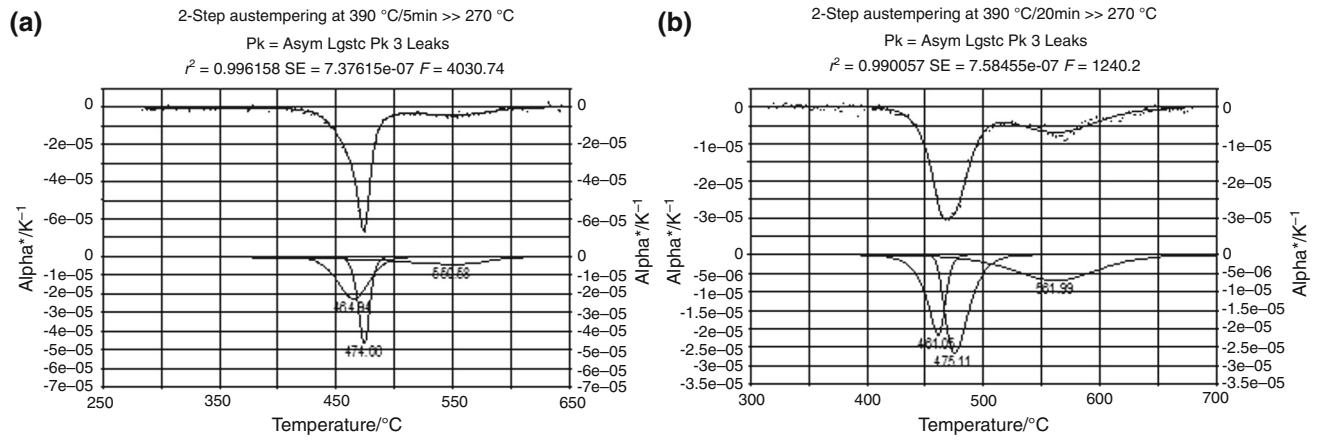

Fig. 6 Deconvolution of dilatometric curves—decomposition after two-step (down) heat treatment; 390 °C/5 min ≫ 270 °C (**a**), 390 °C/20 min ≫ 270 °C (**b**)

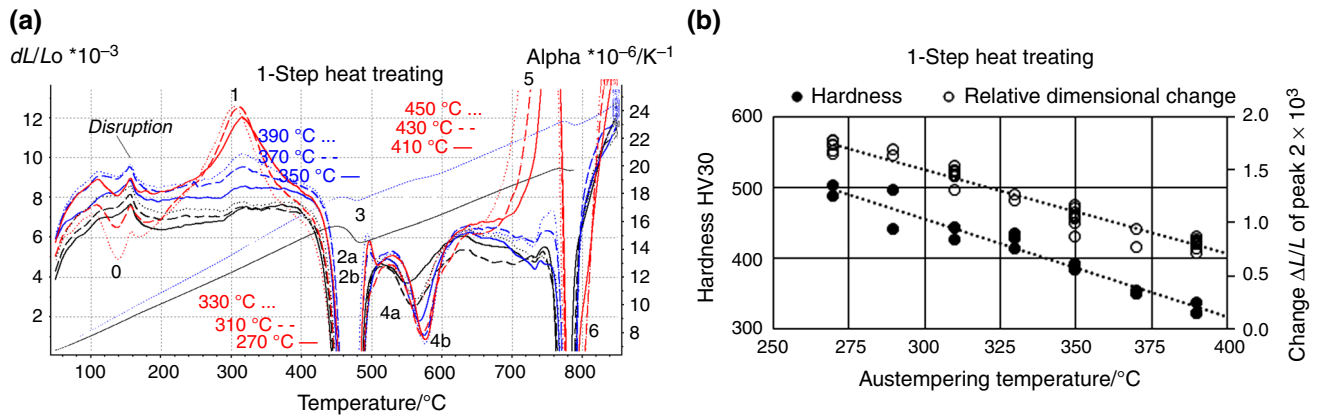

Fig. 7 Enlarged fragments of dilatometric curves of ausferrite decomposition (**a**), relation between HV30 and relative dimensional values of the peak **2** (**b**)

correlated with the magnitude of the effect **0** and increases with the temperature of the isothermal transformation.

In the case of two-step treatment, no martensite tempering effect was observed; effect **1** occurs only when the transformation includes a high austempering temperature step of 390 °C and is lower for step-down heat treatment.

The key effects of ausferrite decomposition are negative effects **2** and **4** (Fig. 7a), which characterize the decomposition process after each ADI treatment. A good correlation was observed between the magnitude of peak **2** and the hardness HV30 (Fig. 7b), indicating that this effect is related to the loss of strength properties of the acicular ferrite. In temperature range of peak **2**, other processes also take place, such as cementite precipitation from supersaturated austenite or coagulation of previously precipitated carbides; therefore, good fitting requires the assumption of a double peak **2a**, **2b** for calculations. It is obvious that the quality of fitting increases with the number of peaks added to the calculations so the assumption of pre-conditions is subjected to the rule—do not multiply peaks over necessity, defined by their physical meaning.

The source of negative value of the main effect of ausferrite tempering is dimensional (volumetric) changes accompanying the mentioned processes as well as high expansion coefficient of the vanishing austenite phase.

Fitting of dilatometric curves after these one- and two-step heat treatment variants when an upper ausferrite is produced is only possible by assuming the presence of additional peak **3**, reflecting the decomposition of austenite saturated with carbon, as evidenced by the positive sign of the effect at high temperature. This is the only case where the decomposition effect of high carbon austenite can be *explicitly* observed in the decomposition curve.

The experiments of the isothermal decomposition of ausferrite at 400, 450, 500 and 550 °C for about 120 min followed by decomposition during heating showed that even after the complete disappearance of effect **2** (450 °C/120 min), peak **4** remains unchanged. Therefore, it is not the result of the decomposition of the products that

preceded it, but that originated in the earlier phase of the decomposition path. Coagulation of the cementite is the only process proceeding in this high temperature range which is mainly the product of the austenite decomposition and indirectly related to its content in the alloy.

Due to the relatively small values of effect **4**, which in case of peak **3** appearance is split into double effects **4a**, **4b**, no satisfactory correlation can be found with carbon-enriched austenite ratio.

Effects **5** and **6** were not analyzed in detail, although they could have an informative significance. Peak **5** appearing only for very high temperature of austempering reflects the ferrite recrystallization and cementite graphitization processes imposed on sharp specific heat (baseline) change in the vicinity of the Curie point. Such an effect proves that processing window is exceeded and eliminates these heat treatment variants. Effect **6** depicts an eutectoid transformation.

Figures 8–10a, b present dependence of values of deconvoluted peaks **2** and **4** found for realized step-up and step-down variants of complex heat treatment.

It is worth noting that highest values and sensitivities of effect **2** and especially effect **4** were obtained for the case step-down heat treatment 390 ≫ 270 °C (Fig. 9b).

Figure 11a shows dependence of dilatometric effects **4** versus **2** calculated for all one-step heat treatment temperature variants with outlined confidence bands at 95% confidence level.

Mechanical properties

The compatibility of relations **4** versus **2** (Fig. 11a) and V_a versus HV30 (Fig. 1b) is a prerequisite for this type of relationships to be used to design optimal heat treatment. This is confirmed in Fig. 11b where the data computed for complex, two-step heat treatment are added. Only step-down heat treatment 390 ≫ 270 °C provides hope for better mechanical properties than one-step heat ADI treatment.

Based on the analysis of the dilatometric test results (Fig. 11b), one- and two-stage heat treatments were performed in the work stand equipped with austenitization

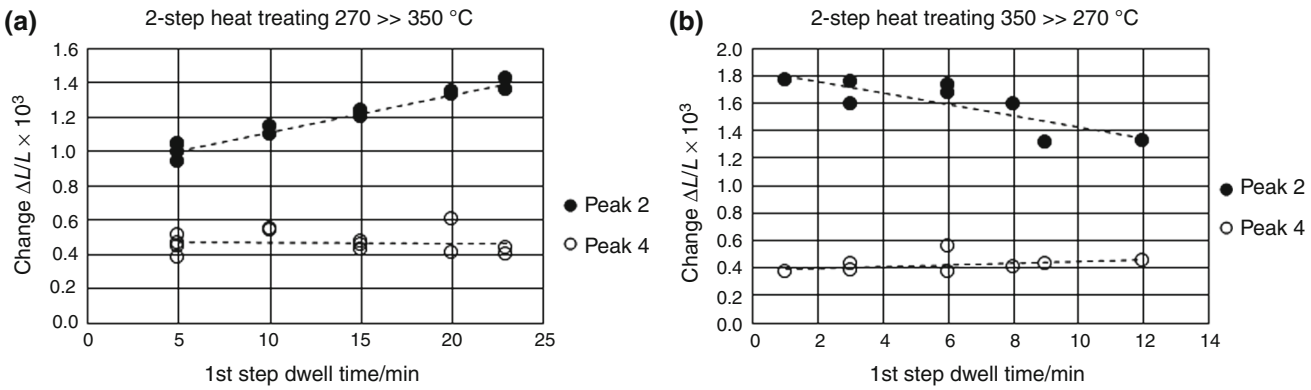

Fig. 8 Dependence of effects **2** and **4** on dwell time of first step of two-step treatment (270 ≫ 350 °C); step-up (**a**), step-down (**b**)

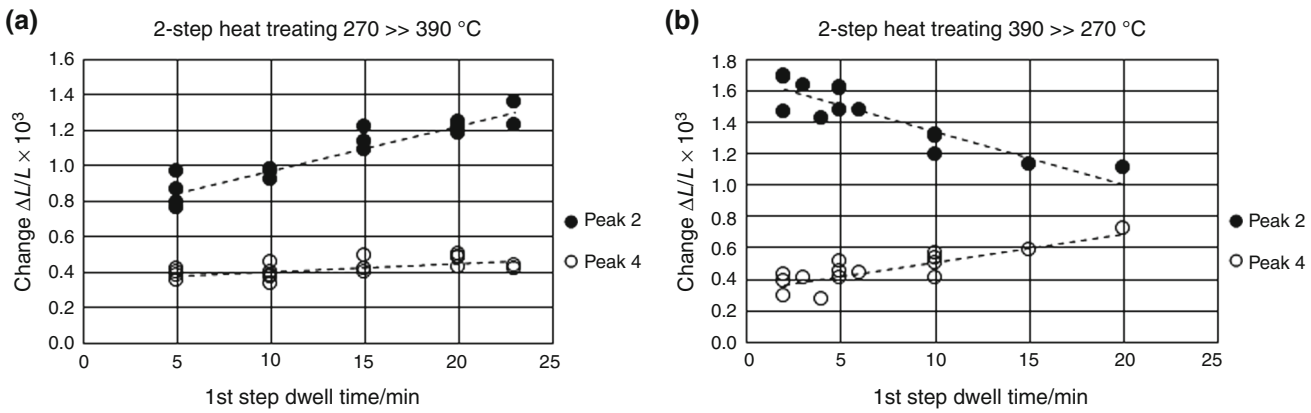

Fig. 9 Dependence of effects **2** and **4** on dwell time of first step of two-step treatment (270 ≫ 390 °C); step-up (**a**), step-down (**b**)

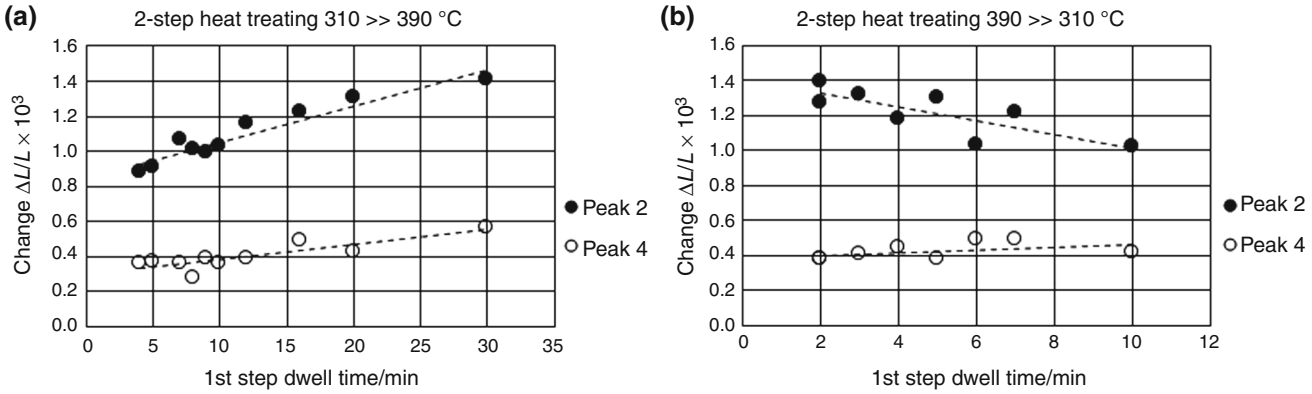

Fig. 10 Dependence of effects **2** and **4** on dwell time of first step of two-step treatment (310 ≫ 390 °C); step-up (**a**), step-down (**b**)

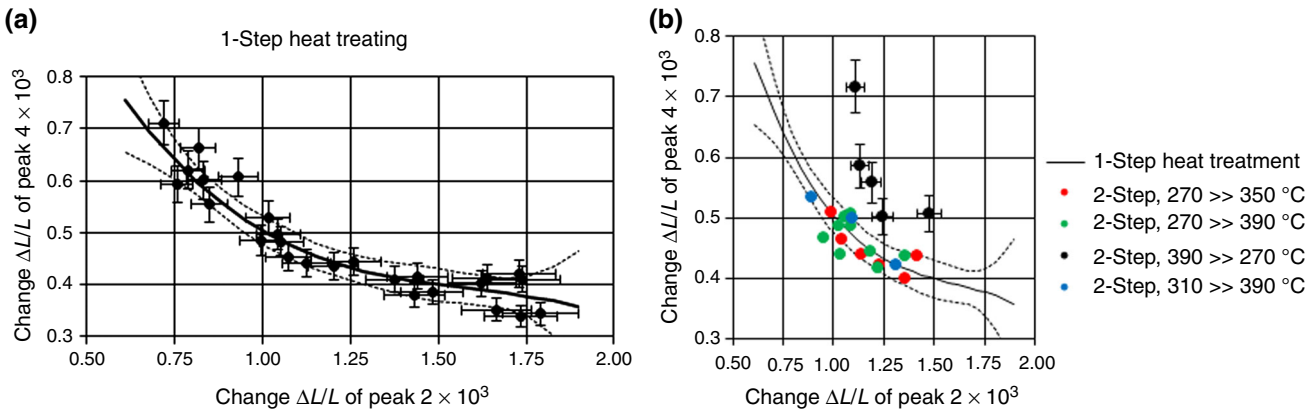

Fig. 11 Relation between dilatometric effects **4** and **2**; for one-step heat treatment (**a**), for two-step heat treatment compared to one-step heat treatment (**b**)

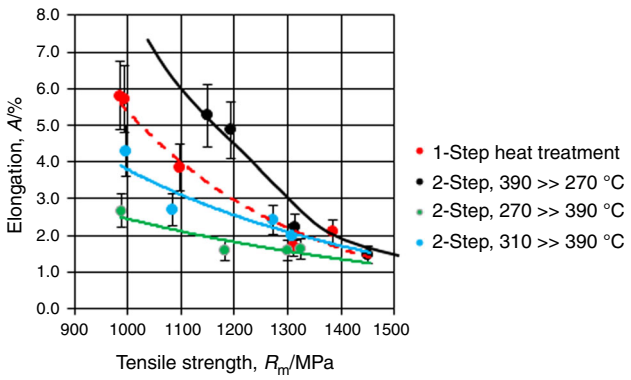

Fig. 12 The relation between elongation A and tensile strength R_m for standard one-step and complex two-step ADI heat treatments

furnace and two salt furnaces to carry out complex austempering, with the possibility of rapid transfer of samples from one bath to another without changing the sample initial temperature.

The samples after selected heat treatment variants were subjected to a static tensile test at room temperature using an EU-20 strength machine. Figure 12 presents dependence of ductility (elongation) on tensile strength R_m for standard one-step and complex two-step ADI heat treatments.

The forecast rightness based on dilatometric analysis has been confirmed; for step-down heat treatments 390 °C/15 min ≫ 270 °C and 390 °C/20 min ≫ 270 °C, mechanical properties have been obtained which cannot be achieved by means of standard one-step ADI heat treatment.

Observations of the fracture surface topography carried out by means of the scanning electron microscopy showed that decohesion mechanism was modified by the heat treatment effect.

The transcrystalline cleavage fracture was observed in material in the as-cast state (Fig. 13a). In the heat-treated material, more of the microregions of the plastic deformation were revealed, while temperature of the isothermal austempering increased from 310 to 390 °C (Fig. 13b, c).

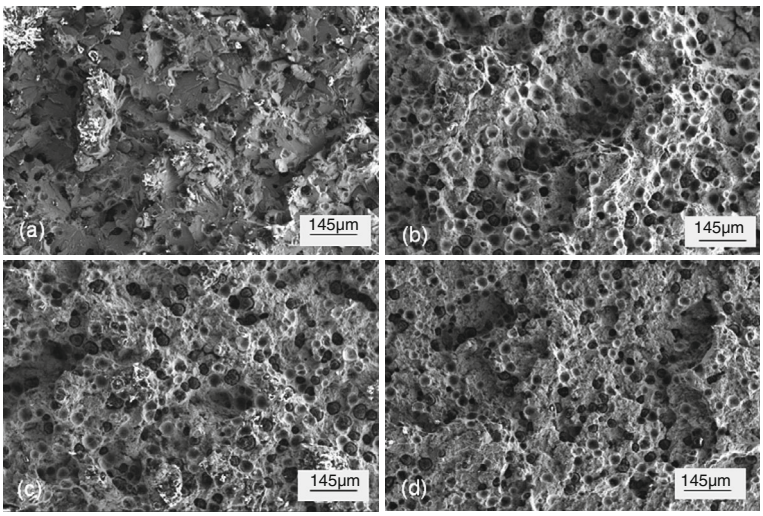

Fig. 13 Morphology of the fracture surface in the examined specimens, SEM; as-cast state, transcrystalline, cleavage fracture in the matrix, with visible decohesion at graphite/matrix interface (**a**), one-step at 310 °C, transcrystalline, mixed cleavage/ductile fracture in the matrix, with visible decohesion at graphite/matrix interface (**b**), one-step at 390 °C, transcrystalline, ductile fracture in the matrix [with small microregion of brittle cracks, with visible decohesion at graphite/matrix interface] (**c**), 2-step (down) 390 ≫ 270 °C, transcrystalline, mixed cleavage/ductile fracture in the matrix, with visible decohesion at graphite/matrix interface (**d**)

On the fracture surface in specimens after heat treatment (310, 390 °C), the dimples characteristic for ductile fracture was visible. Similar morphology to that observed in the specimen austempered at 390 °C, characteristic for ductile fracture, was observed in specimen after two-step heat treatment (Fig. 13d).

The specific features of the fracture surface morphology observed in the examined specimens reflect changes in their fracture mechanism due to alloy microstructure evolution. It was caused, first of all, by effect of heat treatment parameters on change of the microstructure phase composition: rise of products of the isothermal annealing, especially ausferrite, in place of those primary, as pearlite and ferrite. This resulted in the transition of fracture mechanism from that transcrystalline cleavage in as-cast state to transcrystalline ductile or mixed after austempering. The ductile dimples in alloy matrix observed on a fracture surface after heat treatment indicate its local plastic deformation. As it is related to energy absorption, in a macroscope scale, material plasticity increases.

Conclusions

- A method for the precise production and investigation of austempered ductile iron (ADI) has been developed using standard one-step and complex, two-step heat treatments by means of quenching dilatometer.
- Investigations of proceeding phase transformations using differential dilatometric analysis supported by microstructural observations, hardness and austenite volume measurements have been carried out.
- Analysis of the temperature sequence of the ausferrite decomposition in the one-step and two-step ADI was carried out, which allowed for the separation and identification of the effects responsible for acicular ferrite and carbon-enriched austenite decomposition.
- A quantitative relationship was established between basic dimensional effects on the dilatometric differential curve of ausferrite decomposition, which enables prognosis and optimization of the parameters of complex ADI heat treatment variants.
- Evolution of alloy phase composition observed as an effect of the austempering heat treatment led to change in decohesion mechanism from cleavage to ductile which gave a macroscope effect in the form of increase in alloy ductility.
- Microstructure constituents morphology observed as a result of the used heat treatment parameters can have some impact on final macroscope material properties, especially on strength/ductility ratio. However, noticed effect of differences in the retained austenite volume fraction should not be omitted in the procedure of the optimization of the austempering parameters.
- Quantitative dilatometric analysis of the ausferrite decomposition allowed to obtain for the optimal temperature step-down heat treatment 390 °C/15, 20 min ≫ 270 °C/130 min the excellent mechanical properties, unattainable by means of standard 1-step ADI heat treatment.

Acknowledgements This work was financially supported by Polish National Science Centre (NCN) in the Project No. UMO-2013/09/B/ST8/02061.

References

1. Kovacs BV. On the terminology and structure of ADI. Trans Am Foundry Soc. 1994;83:417–20.
2. Chang CH, Shih TS. Ausferrite transformation in austempered alloyed ductile irons. Trans Jpn Foundrym Soc. 1994;13:56–63.
3. Bayati H, Elliott R. The concept of an austempered heat treatment processing window. Int J Cast Met Res. 1999;11:413–7.
4. Vaško A. Influence of transformation temperature on structure and mechanical properties of austempered ductile iron. Acta Metall Slov. 2011;17:45–50.
5. Nofal AA. Advances in metallurgy and applications of ADI. J Metall Eng ME. 2013;2:1–18.
6. Krzyńska A. Searching for better properties of ADI. Arch Foundry Eng. 2013;13:91–6.
7. Korichi S, Priestner R. High temperature decomposition of austempered microstructures in spheroidal graphite cast iron. Mater Sci Technol. 1995;11:901–7.
8. Massone JM, Boeri RE, Sikora JA. Changes in the structure and properties of ADI on exposure to high temperatures. Int J Cast Met Res. 1996;9:79–82.
9. Massone JM, Boeri RE, Sikora JA. Decomposition of high-carbon austenite in ADI. Trans Am Foundry Soc. 1996;96–148:133–7.
10. Nadkarni G, Gokhale S. Elevated temperature microstructural stability of austempered ductile irons. Trans Am Foundry Soc. 1996;96–136:985–94.
11. Baricco M, Franzosi G, Nada R, Battezzati L. Thermal effects due to tempering of austenite and martensite in austempered ductile irons. Mater Sci Technol. 1999;15:643–6.
12. Perez MJ, Cisneros MM, Valdes E, Mancha H, Calderon HA, Campos RE. Experimental study of the thermal stability of austempered ductile irons. J Mater Eng Perform. 2002;11:519–26.
13. Perez MJ, Cisneros MM, Lopez HF, Calderon HA, Valdes E. Microstructural evolution in austempered ductile iron during non-isothermal annealing. Int J Cast Met Res. 2003;16:203–6.
14. Gazda A. Analysis of decomposition processes of ausferrite in copper-nickel austempered ductile iron. J Therm Anal Calorim. 2010;102:923–30.
15. Kutsov A, Taran Y, Uzlov K, Krimmel A, Evsyukov M. Formation of bainite in ductile iron. Mater Sci Eng A. 1999;273–275:480–4.
16. Santos H, Duarte A, Seabra J. Austempered ductile iron with tempered martensite. Int J Cast Met Res. 2002;15:117–24.
17. Morra PV, Bottger PJ, Mittemeijer EJ. Decomposition of iron-based martensite. A kinetic analysis by means of differential scanning calorimetry and dilatometry. J Therm Anal Calorim. 2001;64:905–14.
18. Myszka D. Austenite–martensite transformation in austempered ductile iron. Arch Metall Mater. 2007;52:475–80.
19. Putatunda SK. Development of austempered ductile cast iron (ADI) with simultaneous high yield strength and fracture toughness by a novel two-step austempering process. Mater Sci Eng A. 2001;315:70–80.
20. Hsu C-H, Chuang T-L. Influence of stepped austempering process on the fracture toughness of austempered ductile iron. Metall Mater Trans A. 2001;32A:2509–14.
21. Putatunda SK, Yang J. A novel processing of austempered ductile cast iron (ADI). Mater Sci Forum. 2003;426–432:913–8.
22. Yang J, Putatunda SK. Improvement in strength and toughness of austempered ductile cast iron by a novel two-step austempering process. Mater Des. 2004;25:219–30.
23. Yang J, Putatunda SK. Effect of microstructure on abrasion wear behavior of austempered ductile cast iron (ADI) processed by a novel two-step austempering process. Mater Sci Eng A. 2005;406:217–28.
24. Kaczorowski M, Krzyńska A, Psoda M. Structural investigations of ductile iron after two-step isothermal quenching. Arch Foundry Eng. 2004;4:127–38.
25. Francucci G, Sikora G, Dommarco R. Abrasion resistance of ductile iron austempered by the two-step process. Mater Sci Eng A. 2008;485:46–54.
26. Ravishankar KS, Rao PP, Udupta KR. Improvement in fracture toughness of austempered ductile iron by two-step austempering process. Int J Cast Met Res. 2010;23:330–5.
27. Hernandez-Rivera JL, Garay-Reyes CG, Campos-Cambranis RE, Cruz-Rivera JJ. Design and optimization of stepped austempered ductile iron using characterization techniques. Mater Charact. 2013;83:89–96.
28. Puspitasari A, Puspitasari P. Effect of temperature and time of two-step austempering method on mechanical properties for nodular cast iron. ARPN J Eng Appl Sci. 2016;11:863–6.
29. Rivolta B, Gerosa R. On the non-isothermal precipitation of copper-rich phase in 17-4 PH stainless steel using dilatometric techniques. J Therm Anal Calorim. 2010;102:857–62.
30. Grajcar A, Zalecki W, Skrzypczyk P, Kilarski A, Kowalski A, Kołodziej S. Dilatometric study of phase transformations in advanced high-strength bainitic steel. J Therm Anal Calorim. 2014;118:739–48.
31. Gazda A. Determination of the optimal austempering parameters of Ni–Cu (Mo, Mn) ductile iron based on CCT and TTT diagrams. Prace Inst Odlew. 2016;LVI:133–45.